

## Cross calibration of deformation potentials and gradient-elastic tensors of GaAs using photoluminescence and nuclear magnetic resonance spectroscopy in GaAs/AlGaAs quantum dot structures

E. A. Chekhovich,<sup>1,\*</sup> I. M. Griffiths,<sup>1</sup> M. S. Skolnick,<sup>1</sup> H. Huang,<sup>2</sup> S. F. Covre da Silva,<sup>2</sup> X. Yuan,<sup>2</sup> and A. Rastelli<sup>2</sup>

<sup>1</sup>*Department of Physics and Astronomy, University of Sheffield, Sheffield S3 7RH, United Kingdom*

<sup>2</sup>*Institute of Semiconductor and Solid State Physics, Johannes Kepler University Linz, Altenbergerstr. 69, 4040 Linz, Austria*



(Received 9 May 2018; published 19 June 2018)

Lattice matched GaAs/AlGaAs epitaxial structures with quantum dots are studied at  $T = 4.2$  K under static uniaxial stress applied either along the [001] or [110] crystal directions. We conduct simultaneous measurements of the spectral shifts in the photoluminescence of the bulk GaAs substrate, which relate to strain via deformation potentials  $a$  and  $b$ , and the quadrupolar shifts in the optically detected nuclear magnetic resonance spectra of the quantum dots, which relate to the same strain via the gradient-elastic tensor  $S_{ijkl}$ . Measurements in two uniaxial stress configurations are used to derive the ratio  $b/a = 0.242 \pm 0.008$  in good agreement with previous studies on GaAs. Based on the previously estimated value of  $a \approx -8.8$  eV we derive the product of the nuclear quadrupolar moment  $Q$  and the  $S$ -tensor diagonal component in GaAs to be  $QS_{11} \approx +0.758 \times 10^{-6}$  V for  $^{75}\text{As}$  and  $QS_{11} \approx -0.377 \times 10^{-6}$  V for  $^{69}\text{Ga}$  nuclei. In our experiments the signs of  $S_{11}$  are directly measurable, which was not possible in the earlier nuclear acoustic resonance studies. Our  $QS_{11}$  values are a factor of  $\sim 1.4$  smaller than those derived from the nuclear acoustic resonance experiments [Phys. Rev. B **10**, 4244 (1974)]. The gradient-elastic tensor values measured in this work can be applied in structural analysis of strained III-V semiconductor nanostructures via accurate modeling of their magnetic resonance spectra.

DOI: [10.1103/PhysRevB.97.235311](https://doi.org/10.1103/PhysRevB.97.235311)

### I. INTRODUCTION

Electronic and optical properties of semiconductors depend strongly on the symmetry of the underlying crystal structure [1,2]. Many technologically important semiconductors, such as Si, Ge, GaAs, and InP have high crystal symmetry belonging to the cubic crystal system. Elastic deformation (strain) induced by external stress or internal morphology leads to reduction of the crystal symmetry, resulting in significant modification of the optical and electronic properties. Strain-induced effects not only serve as a tool in studying the physics and structure of semiconductors, but have already found several important applications, including pressure sensors and transducers, as well as MOSFET transistors and semiconductor lasers with improved performance. Semiconductor technologies under development also involve strain effects. One example is quantum information technologies based on semiconductor quantum dots, where strain is used both in self-assembly growth of the quantum dot nanostructures and for tuning their properties [3–8].

The changes in semiconductor electronic properties induced by strain originate from the changes in orientations and overlaps of the electronic orbitals. One manifestation of these changes is in the shifts of the energies of the electronic bands, and in lifting of their degeneracies. In GaAs the strain-induced modification of the electronic structure are commonly described by four parameters—the deformation potentials  $a_c$  and  $a_v$  describe the overall shift of the

conduction and valence bands, respectively, while  $b$  and  $d$  describe lifting of degeneracy and splitting in the valence band (VB) under nonhydrostatic stress. Deformation potentials of GaAs have been measured [9–14] using photoluminescence, photoreflectance, and electroreflectance techniques. The most consistent experimental and theoretical [15–19] results are available for the combination  $a = a_c + a_v$ , which describes the change of the direct band gap in a hydrostatically deformed crystal [20,21]. The largest uncertainty is associated with the individual values of  $a_c$  and  $a_v$ . The  $b$  and  $d$  have been measured as well, although the values quoted in different reports vary by as much as a factor of  $\sim 2$ .

The same strain-induced changes of the electronic bands are responsible for nonzero electric field gradients (EFGs) at the sites of the atomic nuclei (EFGs vanish in an unstrained crystal with cubic symmetry). This effect can be observed as quadrupolar splitting of the nuclear magnetic resonance (NMR) spectra of the nuclei with spin  $I > 1/2$ . The relation between strain and EFG is described by a fourth rank “gradient-elastic” tensor  $S_{ijkl}$ , which can be parametrized by two components  $S_{11}$  and  $S_{44}$  in case of cubic crystal symmetry. By definition,  $S_{ijkl}$  is a phenomenological material parameter which relates microscopic phenomena (atomic scale EFGs) to the macroscopic state of the solid body (elastic strain tensor whose definition ignores the atomic structure of the solid). The need for accurate  $S_{ijkl}$  values have re-emerged recently in view of using NMR for nondestructive structural analysis of nanoscale semiconductor structures [22–28] as well as exploring the effect of nuclear quadrupolar interaction on coherent electron-nuclear spin dynamics in solid state qubits [29–33].

\*e.chekhovich@sheffield.ac.uk

The initial measurements of  $S_{ijkl}$  in various crystal materials used static straining, but their accuracy suffered since quadrupolar spectral shifts were not resolved and could only be observed as broadening of the NMR spectra [34]. In later experiments more reliable measurements were achieved as NMR spectra with resolved quadrupolar satellites could be obtained under static strain [35,36], but in the particular case of GaAs, no accurate estimates of  $S_{ijkl}$  could be derived [37]. Sundfors *et al.* have derived  $S_{ijkl}$  for a wide range of materials [38–41] including GaAs and other III-V semiconductors. The experiments in these studies relied on measuring absorption of the acoustic waves by the nuclei rather than on direct detection of the quadrupolar shifts in NMR spectra. In a more recent study optically detected NMR was measured in a GaAs/AlGaAs quantum well under static bending strain [42]. Quadrupolar shifts were resolved for  $^{75}\text{As}$  and were found to be consistent with the results of acoustic resonance measurement [38,39]. However, the induced deformation was comparable to the built-in strain, the accuracy of strain measurement was limited, and oblique magnetic field configuration meant that individual  $S_{ijkl}$  components were not derived explicitly.

Here we study GaAs/AlGaAs quantum dot (QD) structures and perform simultaneous measurements of optically detected NMR on individual QDs and photoluminescence of free excitons in bulk GaAs substrate in a submicrometer vicinity of the QD. Large elastic deformations exceeding built-in strains by more than an order of magnitude are induced by stressing the samples mechanically. Optically detected NMR reveals spectra with well-resolved quadrupolar satellites, so that quadrupolar shifts are measured with an accuracy of  $\pm 1\%$ . Using the commonly accepted value for deformation potential  $a$ , the energy shifts in the free-exciton photoluminescence of the GaAs substrate are used to measure the magnitude of the same strain field that is probed via QD NMR. From these dual measurements we are able to relate elastic strain to the directly measured nuclear spin quadrupolar shifts and deduce the  $S_{11}$  components of the gradient-elastic tensor of  $^{75}\text{As}$  and  $^{69}\text{Ga}$  in GaAs. Our accurate measurements reveal  $S_{11}$  that are  $\sim 30\%$  smaller than the only other direct measurement based on nuclear acoustic resonance [39]. The  $S_{11}$  constants derived in this work can be used directly in analyzing and predicting the nuclear quadrupolar effects in GaAs-based semiconductor nanostructures. Furthermore, since gradient-elastic tensors describe modification of the electronic orbitals in the vicinity of the nucleus, the accurate experimental  $S_{11}$  values can be used as a reference in fitting the calculated parameters in electronic band-structure modeling [43–45].

## II. STRAIN EFFECTS IN GaAs: DEFINITIONS

The electronic band structure of a bulk crystal can be described by the Luttinger model where the effects of strain are taken into account by the Bir-Pikus Hamiltonian [1,2]. The optical recombination properties of GaAs are determined mainly by the states with momentum  $k \approx 0$  corresponding to the center of the Brillouin zone, which simplifies the analysis. The bottom of the conduction band is twofold degenerate due to the electron spin, and as such remains degenerate under strain. The only effect of strain on the conduction band is an overall energy shift  $a_c \epsilon_h$ , which depends only on the hydrostatic part

of the strain tensor  $\epsilon_h = \epsilon_{xx} + \epsilon_{yy} + \epsilon_{zz}$  (here and throughout the text we use coordinate frame aligned with the cubic crystal axes  $x \parallel [100]$ ,  $y \parallel [010]$ ,  $z \parallel [001]$ ). In case of GaAs  $a_c < 0$ , so that under compressive strain ( $\epsilon_h < 0$ ) the conduction band energy increases.

Without strain, the cubic symmetry of GaAs results in a fourfold degeneracy at the top of the valence band. At small strains the energies of the valence band at  $k = 0$  can be adequately described without coupling to the split-off band, which reduces the model to a  $4 \times 4$  Hamiltonian with a straightforward analytical solution. Strain does not break time reversal symmetry, and thus at most can split the valence band into two states each with a twofold degeneracy. The valence band energy shifts are  $-a_v \epsilon_h \pm \sqrt{b^2 \epsilon_b^2 + \frac{3}{4} b^2 \epsilon_\eta^2 + d^2 \epsilon_s^2}$ , where  $\epsilon_b = \epsilon_{zz} - (\epsilon_{xx} + \epsilon_{yy})/2$  is the “biaxial” component of the shear strain, and we denote  $\epsilon_\eta = \epsilon_{xx} - \epsilon_{yy}$  and  $\epsilon_s^2 = \epsilon_{xy}^2 + \epsilon_{yz}^2 + \epsilon_{xz}^2$ . It is commonly accepted that under compressive hydrostatic strain ( $\epsilon_h < 0$ ) the valence band moves to lower energy, corresponding to  $a_v < 0$  with the sign convention used here [20]. The energy of the photoluminescence photons (measurable experimentally) is the difference of the conduction and valence band energies and can be written as

$$E_{\text{PL}} = E_g + a \epsilon_h \pm \sqrt{b^2 \epsilon_b^2 + \frac{3}{4} b^2 \epsilon_\eta^2 + d^2 \epsilon_s^2}, \quad (1)$$

where  $E_g$  is the direct band gap energy of unstrained GaAs. Under uniaxial compressive stress along  $z$  (characterized by  $\epsilon_{zz} < 0$  and  $\epsilon_{xx} = \epsilon_{yy} > 0$ ) the transition with lower PL energy corresponds to the valence band light holes (LH) with momentum  $j_z = \pm 1/2$ , while higher PL energy corresponds to the heavy holes (HH) with momentum  $j_z = \pm 3/2$ .

In any crystal in equilibrium the electric field at the atomic nucleus site is zero. However, the gradients of the electric field components are not necessarily zero and are described by a symmetric second rank tensor  $V_{ij}$  of the second spatial derivatives of the electrostatic potential  $V$ . In a crystal with cubic symmetry,  $V_{ij}$  vanishes at the nuclear sites, but when the crystal is strained electric field gradients arise and in linear approximation are related to the strain tensor  $\epsilon_{kl}$  via  $V_{ij} = \sum_{k,l} S_{ijkl} \epsilon_{kl}$ . A nucleus with a nonzero electric quadrupolar moment  $eQ$  interacts with the electric field gradients (we follow the convention where elementary charge  $e > 0$  is taken out of the definition of  $Q$ ). In a simplest case of high static magnetic field the effect of the quadrupolar interaction is to split the NMR transition into a multiplet of transitions between the states whose spin projections onto the magnetic field axis differ by  $\pm 1$ . In case of spin  $I = 3/2$  nuclei and static magnetic field directed along the  $z$  axis a triplet of equidistant NMR frequencies is observed with splitting [34,42,46]:

$$\nu_Q = \frac{eQ}{2h} S_{11} \epsilon_b, \quad (2)$$

where  $h$  is the Planck constant and we used Voigt notation for the component of the gradient elastic tensor  $S_{11} = S_{xxxx} = S_{yyyy} = S_{zzzz}$ . (For a detailed derivation see the Appendix A.) Unlike the free-exciton energies measured in PL spectroscopy [Eq. (1)], the shifts measured in NMR spectra [Eq. (2)] are not sensitive to the hydrostatic strain and depend only on

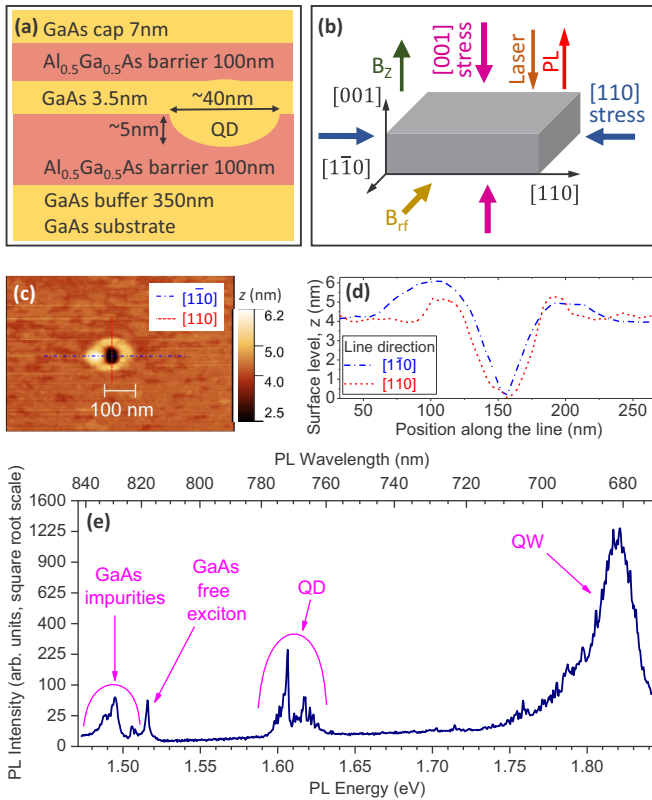


FIG. 1. (a) Sample structure showing the sequence of GaAs and  $\text{Al}_{0.5}\text{Ga}_{0.5}\text{As}$  epitaxial layers. (b) Schematic of the experiment geometry showing orientation of a sample, direction of the static magnetic field  $B_z$ , radio frequency field  $B_{\text{rf}}$ , and the direction of the photoluminescence excitation and collection. External stress is applied either along the  $[001]$  direction or the  $[110]$  direction. (c) AFM image of a sample grown under similar conditions as the studied structure but without overgrowing the  $\text{Al}_{0.5}\text{Ga}_{0.5}\text{As}$  layer with nanoholes. (d) Profiles along the lines in image (c), which are oriented along the  $[001]$  and  $[1\bar{1}0]$  directions. (e) Typical photoluminescence spectrum at  $B_z = 0$  showing emission from the quantum well (QW), a single quantum dot (QD), as well as emission from the GaAs substrate which includes free-exciton emission and impurity-induced recombination. The excitation power is high enough to observe PL of both the ground and excited QD states. Square-root vertical scale is used to reveal weak spectral features.

shear strains of a particular symmetry (described by  $\epsilon_b$ ). This property is exploited in this work to cross calibrate the magnitudes of  $S_{11}$  and deformation potentials.

### III. SAMPLES AND EXPERIMENTAL TECHNIQUES

The structure studied in this work was grown using molecular beam epitaxy. The schematic cross section is shown in Fig. 1(a). The first step in the growth is the deposition of a 350 nm thick buffer GaAs layer onto an undoped  $\sim 0.35$  nm thick  $(001)$ -oriented GaAs wafer. This is followed by the growth of a 100 nm thick bottom barrier  $\text{Al}_{0.5}\text{Ga}_{0.5}\text{As}$  layer. Aluminum droplets are then grown and used to etch nanoholes in the bottom barrier [47,48]. A layer of GaAs with a nominal thickness of 3.5 nm is then deposited, resulting in formation of quantum dots (QDs) due to filling up of the nanoholes, as well

as formation of a quantum well (QW) layer. A 100 nm thick top  $\text{Al}_{0.5}\text{Ga}_{0.5}\text{As}$  barrier layer is then grown, followed by a 7 nm thick GaAs cap layer. A typical atomic force microscopy (AFM) image of a bottom  $\text{Al}_{0.5}\text{Ga}_{0.5}\text{As}$  layer is shown in Fig. 1(c) for a structure grown under similar conditions but without overgrowing the nanoholes. Line scan profiles along the two orthogonal directions are shown in Fig. 1(d) and show that a typical nanohole is  $\sim 40$  nm in diameter and  $\sim 5$  nm deep.

The structure was cleaved into small rectangular parallelepiped pieces with dimensions of  $\sim 0.9 \times 1.5 \times 0.35$  mm along the  $[110]$ ,  $[1\bar{1}0]$ , and  $[001]$  directions, respectively. Three samples were prepared. The first sample is as grown (unstressed). The second sample is glued between two flat titanium surfaces and stressed compressively along the  $[110]$  direction using a titanium screw and nut that press the two titanium surfaces towards each other. The third sample is glued between a titanium flat surface at the bottom and a flat surface of a sapphire window at the top, to be stressed compressively along the  $[001]$  growth direction. All of the samples are studied in a configuration shown in Fig. 1(b). A magnetic field up to 10 T is aligned along the  $z$  axis ( $[001]$ ) within  $\pm 2^\circ$ , which is also the direction of the laser excitation and photoluminescence (PL) collection. For the sample stressed along the  $[001]$  direction, optical excitation and PL propagate through the sapphire window.

All experiments are conducted in a helium bath cryostat at a sample temperature  $\sim 4.2$  K. A small copper coil is mounted close to the sample and is used to generate a radio frequency (rf) magnetic field  $B_{\text{rf}}$  along the  $[1\bar{1}0]$  direction in the NMR experiments. Quantum dot NMR spectra are measured using optical hyperpolarization of the nuclear spins (via circularly polarized laser excitation) and optical detection of the electron hyperfine shifts. The rf field is applied in the absence of optical excitation to ensure the dot is free from electrons and holes that can alter NMR spectra via Knight shifts [49]. The signals of the quadrupolar nuclei are enhanced using “inverse” NMR technique [22]. A detailed description and analysis of the relevant NMR methods has been reported previously [22], and is not repeated here: in this work we use these techniques as a tool that gives an accurate spectral distribution of the resonant frequencies of the nuclei within the volume of an individual quantum dot. The excitation laser is focused into a spot of  $\sim 1$   $\mu\text{m}$  in diameter, so that carriers are generated simultaneously in the QW, the GaAs buffer layer, and the QDs within the area of the laser spot. The photoluminescence signal is collected and analyzed with a grating spectrometer and a charge coupled device (CCD) camera.

A typical broadband PL spectrum measured under HeNe laser excitation (632.8 nm) is shown in Fig. 1(e). Spectral features observed include emission from the QW ( $\sim 1.85$  eV), free-exciton emission of the bulk GaAs buffer and substrate layers ( $\sim 1.515$  eV), impurity-induced PL of bulk GaAs ( $\sim 1.48$ – $1.51$  eV) including bound excitons, as well as recombination involving donor and acceptor states [50–55]. Quantum dot emission is observed at  $\sim 1.60$ – $1.63$  eV and consists of several narrow spectral lines corresponding to different exciton states of a single QD. Since photoluminescence is excited only in a small area of the sample, the spectrum of GaAs free excitons can be used to probe local strain fields in a  $\sim 1$   $\mu\text{m}$  sized spot. Moreover, NMR is detected from the spectral shifts

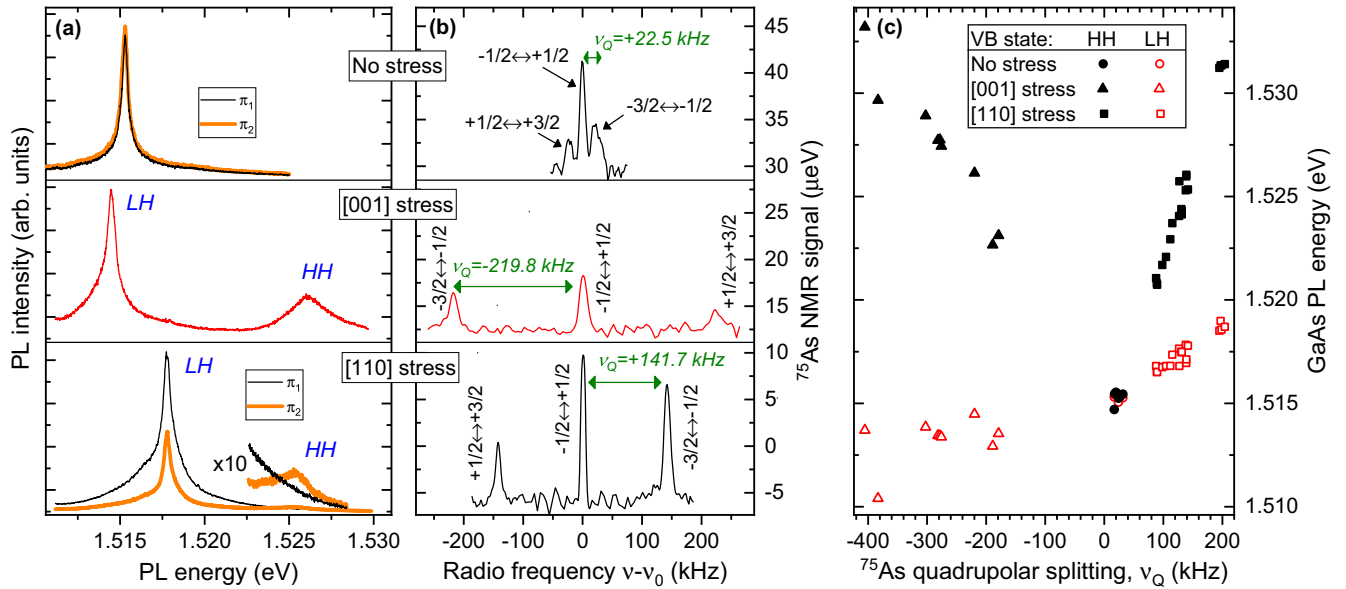


FIG. 2. Effect of strain on bulk GaAs photoluminescence (PL) and quantum dot NMR spectra. (a) Free-exciton PL from a GaAs substrate measured at  $B = 0$  T under excitation with a photon energy  $\sim 1.54$  eV and intensity  $\sim 5 \times 10^6$  W/m<sup>2</sup> in an unstressed sample (top), sample stressed along [001] (middle), and sample stressed along [110] (bottom). In an unstressed sample emission has negligible splitting between peaks detected in two orthogonal linear polarizations ( $\pi_1$ ,  $\pi_2$ ). Stress along [001] splits the luminescence spectrum into two nonpolarized peaks corresponding to emission of light (LH) and heavy (HH) hole excitons. Stress along [110] splits luminescence spectrum into a stronger peak with partial linear polarization corresponding to emission from a predominantly LH exciton, and a weak linearly polarized peak from a predominantly HH exciton (parts of the spectra with  $\times 10$  vertical magnification are shown to reveal the HH peak). (b) Nuclear magnetic resonance spectra of  $^{75}\text{As}$  nuclei measured with  $\sigma^+$  polarized optical excitation at  $B_z = 8$  T ( $\nu_0 \approx 58.46$  MHz) on GaAs/AlGaAs quantum dots in an unstressed (top), [001] stressed (middle), and [110] stressed (bottom) samples. Each NMR spectrum in (b) is measured from the same spot as the corresponding GaAs PL spectrum in (a). Spectra are offset vertically for clarity. Well-resolved NMR triplets arising from quadrupolar effects are observed. In an unstressed sample small quadrupolar shift  $\nu_Q$  is observed due to the residual strain of the GaAs/AlGaAs heterostructure. Under [001] ([110]) stress, the resulting strain shifts the  $-3/2 \leftrightarrow -1/2$  satellite transition to lower (higher) frequency corresponding to negative (positive)  $\nu_Q$ . (c) Energies of HH (solid symbols) and LH (open symbols) bulk GaAs PL peaks plotted against quadrupolar shift  $\nu_Q$  measured in multiple quantum dots in an unstressed (circles), [001]-stressed (triangles), and [110]-stressed (squares) samples. GaAs PL energies and NMR frequencies are derived from the spectra using Lorentzian and Gaussian peak fitting, respectively. Variation of  $\nu_Q$  and PL energies in each sample is due to the inhomogeneity of strain across the sample surface—the exception is the four points at  $\nu_Q \approx +200$  kHz that were measured at an increased stress along [110].

in the QD emission and thus probes an even smaller nanometer-sized part of the optically excited area. In this way it is ensured that GaAs PL spectroscopy and QD NMR probe the same strain field. We also note that while QD exciton energies are sensitive to strain, the achievable stress-induced shifts are comparable to the heavy-light hole splitting induced by breaking of symmetry at heterointerfaces (typically  $\sim 10$  meV in GaAs/AlGaAs QWs [56]), resulting in complex dependence of exciton energies on strain. For that reason calibration of strain in this work is based on free-exciton emission of GaAs which has a straightforward relation to strain [Eq. (1)].

## IV. EXPERIMENTAL RESULTS AND ANALYSIS

### A. Effect of strain on GaAs photoluminescence and nuclear magnetic resonance spectra

Figure 2(a) shows GaAs free-exciton PL spectra measured in three different samples at  $B_z = 0$ , while Fig. 2(b) shows  $^{75}\text{As}$  NMR spectra measured at  $B_z = 8$  T from the QDs in the same optically excited spots as in Fig. 2(a). Since the size of

the optically excited spot is much smaller than the size of the sample, and the stiffness tensors of GaAs and AlAs are very similar [20], all significant variations of strain induced by external stress occur on length scales that are much larger than the studied spot size. As a result, the two types of spectroscopy probe the effect of the same stress field.

Bulk GaAs PL is measured with laser excitation intensity  $\sim 5 \times 10^6$  W/m<sup>2</sup>. On the one hand, it is high enough to saturate the impurity-induced PL and make free-exciton emission dominant, while on the other hand, it is low enough to avoid excessive spectral broadening. In an unstressed sample PL is detected with a variable orientation of linear polarization: the top two spectra in Fig. 2(a) are measured along the orthogonal polarization axes  $\pi_1$ ,  $\pi_2$  and reveal very small polarization degree and a negligible splitting. This is expected for unstrained GaAs PL, since the valence band state at  $k = 0$  is fourfold degenerate. The corresponding NMR spectrum [Fig. 2(b), top] reveals a triplet of lines with a small quadrupolar splitting  $|\nu_Q| \approx 22.5$  kHz, most likely related to the strain arising from the residual lattice mismatch of the GaAs and  $\text{Al}_{0.5}\text{Ga}_{0.5}\text{As}$  layers. Each line of the triplet corresponds to an

individual dipolar nuclear spin transition  $I_z \leftrightarrow I_{z+1}$  as labeled in Fig. 2(b).

For the sample stressed along [001], GaAs free-exciton PL is split into two nonpolarized lines [Fig. 2(a), middle]. This is expected, since deformation along [001] lifts the degeneracy and splits the state at the top of the valence band into a twofold degenerate state with momentum projection  $j_z = \pm 1/2$  corresponding to the light holes (LH), and a twofold degenerate state with  $j_z = \pm 3/2$  corresponding to the heavy holes (HH). The effect of strain is also manifested in NMR through a significantly larger triplet splitting  $|\nu_Q| \approx 219.8$  kHz [Fig. 2(b), middle].

The stress along [110] also splits the fourfold degenerate top of the valence band into two doublets. These are nearly pure heavy and light hole states with momentum quantization axis along [110], and their recombination results in a linearly polarized PL [Fig. 2(a), bottom]. The peak at  $\sim 1.518$  eV is partially linearly polarized and corresponds to the state with predominantly light hole character (LH). By contrast, the peak at  $\sim 1.525$  eV is strongly polarized and corresponds to a predominantly heavy hole state (HH). The intensity of the HH peak is reduced mostly due to the relaxation into the LH state. The NMR triplet splitting [Fig. 2(b), bottom] is also significantly larger than in an unstressed sample with  $|\nu_Q| \approx 141.7$  kHz.

The measurements of GaAs free-exciton PL and  $^{75}\text{As}$  NMR were repeated on multiple spots in all three samples and spectra similar to those shown in Figs. 2(a) and 2(b) were observed. For each spot PL energies and NMR frequencies were derived by fitting the spectral peaks. The resulting summary in Fig. 2(c) shows PL energies of HH (solid symbols) and LH (open symbols) excitons as a function of the quadrupolar splitting  $\nu_Q$  in an unstressed (circles), [001]-stressed (triangles), and [110]-stressed (squares) samples. It can be seen that in the unstressed sample  $\nu_Q$  varies in a small range between 15 and 30 kHz with root-mean-square (rms) deviation of  $(\Delta\nu_Q^2)^{1/2} \approx 4.7$  kHz due to the differences in the residual strains in the individual quantum dots. At the same time GaAs PL peak energies vary in a small range between 1.5145 and 1.5155 eV most likely due to the local residual strains arising from crystal imperfections. The spectral shifts in the stressed samples are significantly larger than the random variations in the unstressed sample. There is a clear trend in Fig. 2(c) that larger quadrupolar shifts are correlated with larger GaAs PL energy shifts. On the other hand, the stress-induced spectral shifts (both in PL and NMR) vary across the surface area of the sample, since nonuniform contact between the sample and the titanium stress mount leads to spatial nonuniformity of the stress and strain fields. However, these nonuniformities have characteristic lengths much larger than the laser excitation spot, so that the strain detected in optical PL and NMR spectra can be treated as homogeneous for each individual spot.

For the purpose of quantitative analysis it is convenient to replot the data of Fig. 2(c) in a different form. This is shown in Fig. 3 where the average energy of LH and HH (solid symbols, left scales) as well as the splitting of the LH and HH (open symbols, right scales) are plotted as a function of  $\nu_Q$  for the [001]-stressed (a) and [110]-stressed (b) samples.

In case of the [001]-stressed sample [Fig. 3(a)], the average energy of LH and HH shows significant random variations.

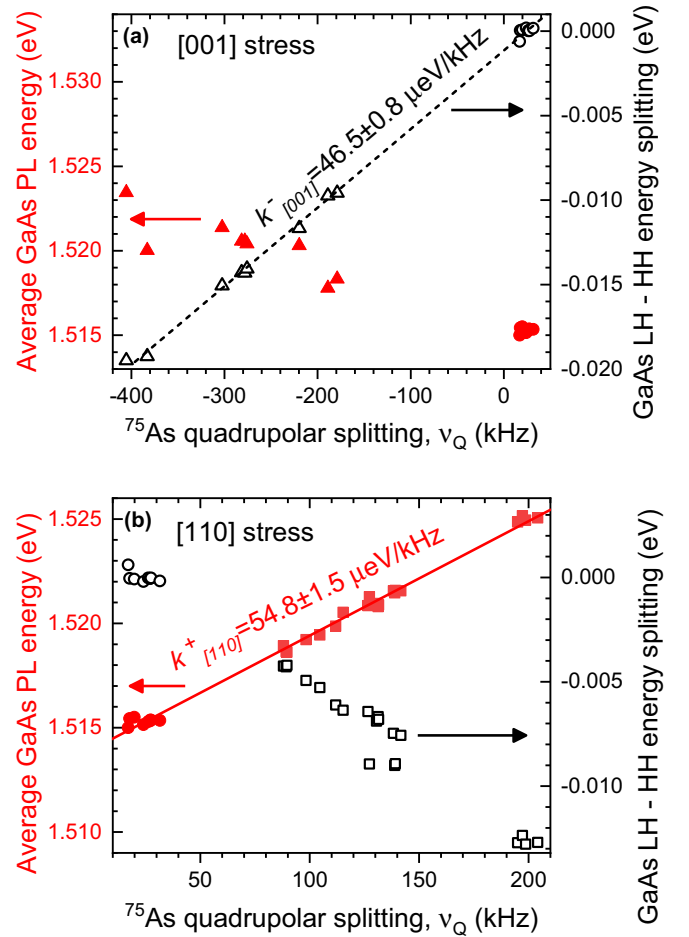


FIG. 3. Data of Fig. 2(c) plotted in terms of the arithmetic average PL energy of the LH and HH excitons (solid symbols, left scales) and the difference of the LH and HH exciton PL energies (open symbols, right scales) as a function of  $^{75}\text{As}$  quadrupolar shift  $\nu_Q$ . (a) Results for the unstressed (circles) and [001]-stressed (triangles) samples. LH-HH splitting is well described by a linear function with a slope  $k_{[001]}^- = 46.5 \pm 0.8 \mu\text{eV/kHz}$  (dashed line). (b) Results for the unstressed (circles) and [110]-stressed (squares) samples. The average LH-HH PL energy is well described by a linear function with a slope  $k_{[110]}^+ = 54.8 \pm 1.5 \mu\text{eV/kHz}$  (solid line).

By contrast, the LH-HH splitting is very well described by a linear dependence on  $\nu_Q$ : the best fit is shown by a dashed line in Fig. 3(a) and the rms fit residual  $(\Delta\nu_Q^2)^{1/2} \approx 4.9$  kHz is essentially the same as the dot-to-dot variation in an unstressed sample. The fitted slope is  $k_{[001]}^- = 46.5 \pm 0.8 \mu\text{eV/kHz}$  (95% confidence interval), which can be rewritten in dimensionless units as  $k_{[001]}^-/h = (1.12 \pm 0.02) \times 10^7$ . The intercept point is at  $\nu_Q \approx 24.6$  kHz which characterizes the average constant offset in the magnitudes of strain inside the QD and in the underlying GaAs buffer layer due to the lattice mismatch at the GaAs/AlGaAs interfaces of the dot. The situation is reversed for the sample stressed along [110] as shown in Fig. 3(b). While the LH-HH splitting shows variations, the dependence of the average LH and HH recombination energies is well described by a linear function (solid line) with a fitted slope  $k_{[110]}^+ = 54.8 \pm 1.5 \mu\text{eV/kHz}$  (rms deviation from the fit is  $(\Delta\nu_Q^2)^{1/2} \approx 4.2$  kHz), or in dimensionless units  $k_{[110]}^+/h =$

$(1.32 \pm 0.04) \times 10^7$ . As we show below, such a difference between the cases of [001]-stressed and [110]-stressed samples is not a coincidence. With some basic assumptions about the spatial distribution of strain in the stressed samples the measured  $k_{[001]}^-$  and  $k_{[110]}^+$  values are used to derive the gradient elastic tensor component  $S_{11}$  as show in Sec. IV D. Prior to this derivation, in the next subsections we present analysis of the properties of the gradient-elastic tensor that require no assumptions about strain configuration.

It is worth noting that rigorous analysis of bulk GaAs PL spectra requires taking into account effects such as electron-hole exchange interaction and polaritons [55]. However, these effects are of the order of  $\sim 0.25$  meV, which is significantly smaller than the strain induced spectral shifts observed here. More importantly, it has been shown that the strain-induced spectral shifts of all the PL components are well described by the free electron and hole deformation potentials [55]. Since our subsequent analysis relies only on the ratios of the strain-induced PL and NMR spectral shifts (rather than absolute GaAs PL energies), it is sufficient to use a simplified “free-exciton” description of the GaAs PL ignoring polariton effects.

### B. Measurement of the sign of the S-tensor components

We now show how the sign of the gradient-elastic tensor can be determined directly, as long as it is possible to identify the spin projections of the nuclear spin states corresponding to each NMR transition. The nuclear spin states can be identified from the hyperfine interaction effects, if the sign of the electron spin polarization is known. In order to define the sign of the electron spin polarization we start by considering the signs of the carrier  $g$  factors. The electron  $g$  factor in the studied QDs [57], as well as in thin GaAs/AlGaAs quantum wells [58], is small and the shifts of the excitonic levels induced by magnetic field along the growth axis are dominated by the hole Zeeman effect. The sign of the hole  $g$  factor [57,58] is such that at positive magnetic field  $B_z > 0$  the exciton with a positive (negative) hole momentum projection  $j_z = +3/2$  ( $-3/2$ ) labeled  $\uparrow$  ( $\downarrow$ ) has higher (lower) energy. In order to be optically active the high- (low-) energy exciton must have electron spin projection  $s_z = -1/2$  ( $+1/2$ ) denoted  $\downarrow$  ( $\uparrow$ ). Figure 4(a) shows PL spectra of a neutral exciton in a typical QD at  $B_z = 8$  T measured under  $\sigma^+$  and  $\sigma^-$  optical excitation at  $\sim 1.65$  eV. Each PL spectrum is a doublet of optically allowed (“bright”) excitons. Based on the sign of the hole  $g$  factor the high- (low-) energy Zeeman component is attributed to recombination of a  $\uparrow\downarrow$  ( $\downarrow\uparrow$ ) exciton.

Two effects are observed under circularly polarized excitation in Fig. 4(a): (i) the emission intensity of the high- (low-)energy Zeeman component is enhanced under  $\sigma^+$  ( $\sigma^-$ ) excitation, and (ii) the spectral splitting increases (decreases) under  $\sigma^+$  ( $\sigma^-$ ) excitation due to the buildup of nuclear spin polarization. These two effects are related: to understand their origin we first consider the case of  $\sigma^+$  excitation [Fig. 4(b)], which generates predominantly  $\uparrow\downarrow$  excitons. During repeated optical excitation the  $s_z = -1/2$  electrons transfer their polarization to the nuclei of the dot via the flip-flop process [59] enabled by the hyperfine interaction whose Hamiltonian is  $\hat{H}_{\text{hf}} = A(\hat{\mathbf{s}} \cdot \hat{\mathbf{I}})$ . Since the flip-flops are spin conserving, the nuclei become predominantly polarized into the states with negative spin  $I_z < 0$ . The net nuclear spin polarization

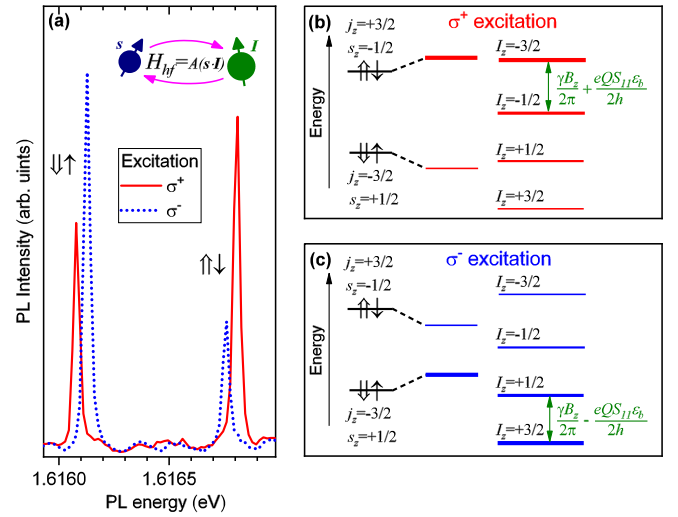


FIG. 4. Derivation of the sign of the gradient elastic tensor. (a) Photoluminescence spectra of a QD neutral exciton measured at  $B_z = 8$  T under  $\sigma^+$  (solid line) and  $\sigma^-$  (dashed line) polarized excitation at  $\sim 1.65$  eV. The  $\sigma^+$  excitation predominantly populates the exciton state with hole momentum  $j_z = +3/2$  ( $\uparrow$ ) and electron spin  $s_z = -1/2$  ( $\downarrow$ ), while  $\sigma^-$  excitation predominantly populates the  $\downarrow\uparrow$  exciton. Electron spin  $s$  can be transferred to a nuclear spin  $I$  via hyperfine interaction (inset) resulting in dynamic nuclear polarization, which in turn leads to hyperfine shifts of the exciton transitions. (b) Schematic of spin effects under  $\sigma^+$  excitation which increases population of the  $s_z = -1/2$  excitons (thicker horizontal line) and reduces population of the  $s_z = +1/2$  exciton (thinner line). Dynamic nuclear polarization enhances the populations of the  $I_z = -3/2$  and  $I_z = -1/2$  nuclear spin states. This is observed as a hyperfine shift of the  $s_z = -1/2$  excitons to higher energy and enhanced amplitude of the  $-3/2 \leftrightarrow -1/2$  NMR transition with frequency  $\frac{\gamma B_z}{2\pi} + \frac{eQ}{2h} S_{11} \epsilon_b$ . (c) Excitation with  $\sigma^-$  light leads to the opposite sign of electron and nuclear spin polarizations, enhancing the  $+1/2 \leftrightarrow +3/2$  NMR transition at frequency  $\frac{\gamma B_z}{2\pi} - \frac{eQ}{2h} S_{11} \epsilon_b$ . By matching the signs of the exciton spectral shifts in (a) and the sign of the NMR spectral shifts [cf. Fig. 2(b)] it is possible to deduce the sign of the gradient elastic tensor component  $S_{11}$  (see Sec. IV B).

back-acts on the electron spin via Overhauser field originating from the same hyperfine interaction [60,61]. The electron hyperfine constant  $A$  is positive for Ga and As nuclei due to their positive gyromagnetic ratios  $\gamma > 0$ , whereas hole hyperfine interaction is an order of magnitude smaller and can be neglected here [62]. As a result the  $\uparrow\downarrow$  exciton shifts to higher energy under  $\sigma^+$  excitation. In a similar manner, under  $\sigma^-$  excitation [Fig. 4(c)] the population of the  $\downarrow\uparrow$  exciton is enhanced, and it also shifts to higher energy since now both  $s_z$  and  $I_z$  are positive. This is indeed observed experimentally as shown in Fig. 4(a): the Zeeman component whose intensity is enhanced by circularly polarized excitation always shifts to higher energy. This observation confirms the positive sign of  $A$  and that the spin flip-flops are the source of dynamic nuclear polarization. Taking also into account the signs of the electron and hole  $g$  factors, we conclude that circularly polarized excitation that enhances the high- (low-)energy exciton population and labeled here  $\sigma^+$  ( $\sigma^-$ ),

populates predominantly the nuclear spin states with negative (positive) projection  $I_z$ .

For the NMR spectra measured with  $\sigma^+$  optical excitation the population of the  $I_z = -3/2$  and  $I_z = -1/2$  states is enhanced as discussed above. As a result the amplitude of the  $-3/2 \leftrightarrow -1/2$  satellite NMR peak exceeds the amplitude of the  $+1/2 \leftrightarrow +3/2$  satellite [63]. The spectra of Fig. 2(b) were measured under  $\sigma^+$  optical excitation (i.e., excitation that enhances the intensity of the high energy Zeeman exciton component). For the case of compressive stress along [001] the  $-3/2 \leftrightarrow -1/2$  NMR peak has a lower frequency than the  $-1/2 \leftrightarrow +1/2$  central peak [middle spectrum in Fig. 2(b)], corresponding to  $\nu_Q < 0$ . The quadrupolar shift  $\nu_Q$  is related to strain via Eqs. (A9) and (A10) and we find that  $\nu_Q = \frac{eQ}{2h} S_{11} \epsilon_b < 0$  in this experiment. In case of [001] compression  $\epsilon_b < 0$ , and since the quadrupolar moment of  $^{75}\text{As}$  is positive [64]  $Q > 0$ , we finally concluded that  $S_{11} > 0$  for  $^{75}\text{As}$ .

While in the above calculations we assumed  $B_z > 0$ , the opposite assumption  $B_z < 0$  leads to the same conclusions about the signs of the gradient elastic tensor components  $S_{11}$ . Finally, we note that in previous work on InGaAs/GaAs [22] and GaAs/AlGaAs [57] QDs, the shift of the  $-3/2 \leftrightarrow -1/2$  satellite peak to lower frequency was arbitrarily assigned a positive  $\nu_Q$  value since the sign of  $S_{11}$  was undefined. By contrast, in the present work the sign of  $\nu_Q$  is strictly determined by Eqs. (2), (A9), and (A10) and the signs of  $S_{11}$  and  $Q$ .

### C. Measurement of the ratio of the electric field gradients on As and Ga lattice sites

Measurement of NMR via optical detection of the hyperfine shifts in the PL spectra of a quantum dot guarantees that only the nuclei of a single quantum dot contribute to the NMR spectrum. Thus if NMR spectrum is measured on As and Ga nuclei of the same quantum dot, one can ensure that the nuclei of the two isotopes belong to the same nanoscale volume and probe the same strain field. The equivalence of strain for cations and anions follows from the requirement of the integrity of the sample and its crystal structure. Mathematically this means that the displacement fields  $\vec{u}(x, y, z)$  of the cation and anion sublattices cannot differ by more than a small fraction of the crystal lattice constant. And since  $\vec{u}(x, y, z)$  is a smooth function, the strain tensor composed of its derivatives [Eq. (A1)] is constrained to have similar values for the two sublattices. According to Eq. (2), the ratio of the quadrupolar shifts of the two isotopes is simply  $\nu_Q^{69\text{Ga}}/\nu_Q^{75\text{As}} = (Q^{69\text{Ga}} S_{11}^{69\text{Ga}})/(Q^{75\text{As}} S_{11}^{75\text{As}})$  and does not depend on the actual strain magnitude  $\epsilon_b$ . Figure 5(a) shows NMR spectra of  $^{69}\text{Ga}$  (top) and  $^{75}\text{As}$  (bottom) measured on the same quantum dot at  $B_z = 5.5$  T using  $\sigma^+$  optical excitation. Both isotopes have spin  $I = 3/2$  giving rise to the well-resolved NMR triplets with different quadrupolar splittings  $\nu_Q$ . We note that the satellite peak with higher amplitude, corresponding to the  $-3/2 \leftrightarrow -1/2$  transition, appears on the low (high) frequency side for Ga (As) implying opposite signs of  $\nu_Q$  and hence opposite signs of  $Q S_{11}$  for the two isotopes. Since  $S_{11} > 0$  for  $^{75}\text{As}$  and  $Q > 0$  for both  $^{69}\text{Ga}$  and  $^{75}\text{As}$  we conclude that  $S_{11} < 0$  for  $^{69}\text{Ga}$ . Since EFGs are very similar and  $Q > 0$  for both Ga isotopes we deduce that  $S_{11} < 0$  for

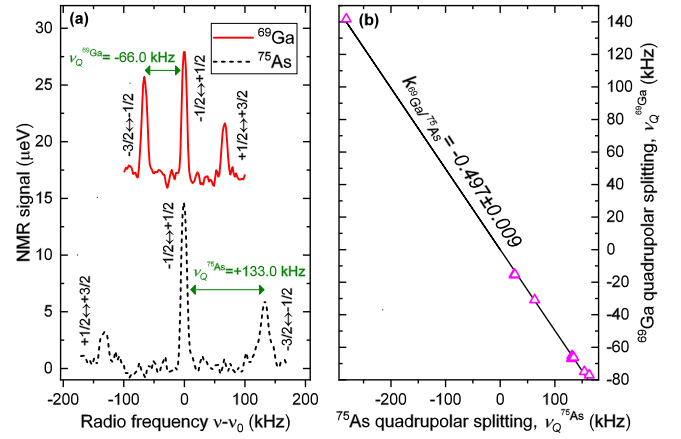


FIG. 5. (a) NMR spectra of a single quantum dot measured at high magnetic field  $B_z \approx 5.5$  T on  $^{75}\text{As}$  nuclei ( $\nu_0 \approx 40.27$  MHz, dashed line) and  $^{69}\text{Ga}$  nuclei ( $\nu_0 \approx 56.46$  MHz, solid line). Both isotopes are spin-3/2 and exhibit well resolved quadrupolar triplets with different splittings  $\nu_Q$ . Spectra are offset vertically for clarity. (b) Dependence of the  $^{69}\text{Ga}$  quadrupolar splitting  $\nu_Q^{69\text{Ga}}$  on the  $^{75}\text{As}$  splitting  $\nu_Q^{75\text{As}}$  measured on different individual quantum dots in an unstressed sample as well as in samples stressed along [001] or [110] crystal axes (symbols). Linear fitting is shown by the solid line and its slope  $k^{69\text{Ga}/75\text{As}} = -0.497 \pm 0.009$  gives an estimate of the ratio  $(Q^{69\text{Ga}} S_{11}^{69\text{Ga}})/(Q^{75\text{As}} S_{11}^{75\text{As}})$  between the products of the quadrupolar moments  $Q$  and gradient elastic tensor components  $S_{11}$  of  $^{69}\text{Ga}$  and  $^{75}\text{As}$  in GaAs.

$^{71}\text{Ga}$  as well. Similar measurements of  $^{69}\text{Ga}$  and  $^{75}\text{As}$  NMR were conducted on a subset of quantum dots used for Figs. 2 and 3 in an unstressed and stressed samples and are summarized in Fig. 5(b), where  $\nu_Q^{69\text{Ga}}$  is shown as a function of  $\nu_Q^{75\text{As}}$  by the symbols. The linear fit is shown by the line and yields the slope  $k^{69\text{Ga}/75\text{As}} = (Q^{69\text{Ga}} S_{11}^{69\text{Ga}})/(Q^{75\text{As}} S_{11}^{75\text{As}}) = -0.497 \pm 0.009$  (95% confidence level). The rms fitting residual in terms of  $\nu_Q^{69\text{Ga}}$  is only  $\approx 1.9$  kHz confirming the validity of the linear model and hence confirming that Ga and As nuclei inside a dot are subject to the same strain. Taking the values of quadrupolar moments [64]  $Q^{69\text{Ga}} = 0.171 \times 10^{-28}$  m<sup>2</sup> and  $Q^{75\text{As}} = 0.314 \times 10^{-28}$  m<sup>2</sup> we calculate for the ratio of the components of the gradient elastic tensors:  $S_{11}^{69\text{Ga}}/S_{11}^{75\text{As}} = -0.912$ , so that the magnitude of the strain-induced EFG is found to be smaller at the gallium sites.

### D. Derivation of the gradient-elastic tensor component $S_{11}$ in GaAs

We now discuss how simultaneous measurements of GaAs free-exciton PL and QD NMR presented in Sec. IV A can be used to calibrate the fundamental material parameters of GaAs. First we consider the case of a sample stressed along the [001] direction. If the stress is produced by applying a uniform  $z$ -oriented pressure to the top and bottom (001) surfaces of the sample, the resulting strain has a very simple configuration where  $\epsilon_h$  and  $\epsilon_b$  are finite, while  $\epsilon_\eta$  and  $\epsilon_\varsigma$  vanish for symmetry reasons ( $\epsilon_{xx} = \epsilon_{yy}$  and  $\epsilon_{xy} = \epsilon_{yz} = \epsilon_{zx} = 0$ ). In this case, according to Eq. (1) the splitting between the LH and HH PL transition energies is simply  $2|b\epsilon_b|$ . Since both the LH-HH

exciton splitting and the NMR shift [Eq. (2)] now depend only on  $\epsilon_b$ , their ratio can be taken to eliminate  $\epsilon_b$  and we find

$$\frac{e}{h} k_{[001]}^- = -\frac{4b}{QS_{11}}, \quad (3)$$

where the minus sign is added to account for the fact that the PL of the LH exciton has a lower energy at  $\epsilon_b < 0$ . The  $k_{[001]}^-$  has been measured experimentally for  $^{75}\text{As}$  [see Fig. 3(a) and Sec. IV A].

In a real sample, the pressure on the surfaces of the sample is not necessarily uniform and aligned to the  $z$  axis. In this case Eq. (3) holds only at the geometrical center of the top (001) surface (for symmetry reasons), while away from the center the nondiagonal strain components may arise leading, e.g., to  $\epsilon_s \neq 0$ . According to Eqs. (1) and (2) the effect of finite  $\epsilon_s$  or  $\epsilon_\eta$  would be to induce an additional splitting of the HH and LH free excitons in the GaAs substrate without affecting the QD NMR spectral splitting  $\nu_Q$ , in which case the dependence of the LH-HH splitting on  $\nu_Q$  would no longer be linear when measured over the surface of the sample. In experiment, multiple spots of the [001]-stressed sample, both at the center of the sample surface and close to the edges were investigated. The strain can be seen to vary significantly across the sample surface:  $\nu_Q$  is found to range from  $-400$  to  $-180$  kHz [Fig. 3(a)] indicating variation of  $\epsilon_b$ , while the spread in the average GaAs PL energies [full triangles in Fig. 3(a)] indicates variation of  $\epsilon_h$ . On the other hand, the resulting dependence of the LH-HH splitting on  $\nu_Q$  is still well described by a linear function [open triangles and dashed line in Fig. 3(a)]. This can only be if  $\epsilon_s$  and  $\epsilon_\eta$  are small indicating that the stress configuration in the studied sample can be considered as uniaxial along [001], with only the stress magnitude exhibiting lateral variations. Consequently, the experimentally measured ratio  $k_{[001]}^- = 46.5 \pm 0.8 \mu\text{eV}/\text{kHz}$  describes the relation of the fundamental parameters  $b$  and  $S_{11}$  of GaAs according to Eq. (3).

We now consider the case of a sample stressed along the [110] direction. If the stress is produced by applying a uniform pressure along [110] to the (110) surfaces of the sample the resulting strain will have nonzero  $\epsilon_h$ ,  $\epsilon_b$ , as well as  $\epsilon_s$ , arising from the  $\epsilon_{xy}$  component. (Recall that  $x$  and  $y$  axes are aligned along [100] and [010], respectively, so that  $\epsilon_{xy} \approx \epsilon_{xx} = \epsilon_{yy}$  under uniform stress along [110].) Even in an ideal case the GaAs PL energies [Eq. (1)] under [110] stress involve the  $d^2\epsilon_s^2$  term, making it difficult to relate to the NMR shifts given by Eq. (2). In a real sample, the nondiagonal shear strain  $\epsilon_{xy}$  is not necessarily constant across the surface of the sample and  $\epsilon_\eta$  is not necessarily zero due to the inevitable nonuniformities of the stress induced by the titanium strain mount. This is evidenced in Fig. 3(b) where the LH-HH splitting (open squares) is seen to deviate considerably from a linear dependence on  $\nu_Q$ , which is proportional only to  $\epsilon_b$ .

However, it is possible to eliminate the effect of the unknown shear strain components  $\epsilon_s$ ,  $\epsilon_\eta$  in a [110]-stress configuration. For that we notice that the top (001) surface of the sample which is studied optically is free from external stress (traction free). As a result, the boundary conditions dictate [65] that three of the components of the mechanical stress tensor vanish  $\sigma_{zx} = \sigma_{zy} = \sigma_{zz} = 0$ , and the only nonzero components are  $\sigma_{xx}$ ,  $\sigma_{yy}$ ,  $\sigma_{xy}$ . Writing down the strain-stress relation one can easily verify that in a GaAs crystal (cubic symmetry), the

ratio of the biaxial and hydrostatic strains at the free (001) surface does not depend on the actual  $\sigma_{xx}$ ,  $\sigma_{yy}$ ,  $\sigma_{xy}$  values and equals  $\epsilon_b/\epsilon_h = \frac{\sigma_{xx} + \sigma_{yy}}{2c_{12} + c_{11}} / \frac{\sigma_{xx} + \sigma_{yy}}{2c_{12} - 2c_{11}} = \frac{2c_{12} + c_{11}}{2c_{12} - 2c_{11}} \approx -1.742$ , where  $c_{11}$  and  $c_{12}$  are the stiffness constants of GaAs [21]. Now we use this relation to express  $\epsilon_b$  through  $\epsilon_h$  in Eq. (2) to make quadrupolar shift  $\nu_Q$  depend only on  $\epsilon_h$ . Since the average LH-HH shift of the GaAs PL energy  $a\epsilon_h$  also depends only on  $\epsilon_h$  [Eq. (1)] it can be related to  $\nu_Q$  by eliminating the strain to find

$$\frac{e}{h} k_{[110]}^+ = \frac{4a}{QS_{11}} \frac{c_{12} - c_{11}}{2c_{12} + c_{11}}. \quad (4)$$

The solid symbols and the line in Fig. 3(b) demonstrate that the average GaAs PL energy is indeed a linear function of  $\nu_Q$ , confirming the invariance of  $\epsilon_b/\epsilon_h$  at the surface of the studied sample. Thus Eq. (4) relates the  $a$  and  $S_{11}$  parameters through the experimentally measured value  $k_{[110]}^+ = 54.8 \pm 1.5 \mu\text{eV}/\text{kHz}$ .

Since the absolute values of stress and strain are not measured in our experiment, the results presented above can be used to estimate the ratios of the GaAs parameters. The absolute value of a parameter can then be estimated by taking the values of other parameters from previous studies.

The elementary charge  $e$  and the Planck constant  $h$  are known with very high accuracy. The stiffness constants of GaAs  $c_{11}$  and  $c_{12}$  are also known with a good accuracy. While  $c_{11}$  and  $c_{12}$  in GaAs exhibit some temperature dependence, the ratio  $c_{11}/c_{12}$  used in our analysis is reported to be nearly invariant from cryogenic to room temperature [66]. Here we use the  $c_{11}$ ,  $c_{12}$  values at 300 K from Ref. [21]. This leaves three GaAs parameters: the deformation potentials  $a = (a_c + a_v)$ ,  $b$ , and the  $QS_{11}$  product of  $^{75}\text{As}$ . Since there are two experimentally measured ratios [Eqs. (3) and (4)], these three parameters can be linked by two independent relations.

One of the relations can be obtained by dividing Eqs. (3) and (4) to eliminate  $QS_{11}$  which gives the ratio of the deformation potentials:

$$\begin{aligned} \frac{b}{a} &= \frac{k_{[100]}^-}{k_{[110]}^+} \frac{c_{12} - c_{11}}{2c_{12} + c_{11}} \\ &= (0.844 \pm 0.027) \frac{c_{12} - c_{11}}{2c_{12} + c_{11}} = 0.242 \pm 0.008, \quad (5) \end{aligned}$$

where the error estimate is purely due to the experimental uncertainty in  $k_{[100]}^-$  and  $k_{[110]}^+$  and there can be an additional error due to the  $\sim \pm 2\%$  uncertainty in the  $c_{11}$ ,  $c_{12}$  values. Our estimate of  $b/a$  is in excellent agreement with the ratio derived from the recommended [20,21] values of  $a$  and  $b$  based on a number of independent experimental and theoretical studies. Such agreement supports the validity of our experimental method based on relating PL and NMR spectral shifts. The estimates derived in this work are summarized in Table I together with the results of the earlier work.

For the second relation we use Eq. (4) to link the deformation potential  $a$  with the component of the gradient elastic tensor  $S_{11}$ . The variation of the GaAs fundamental gap under hydrostatic strain characterized by  $a = a_c + a_v$  has been studied experimentally by several authors [3–7]. There is some variation, but most experiments as well as calculations [16] are consistent and it is commonly accepted [20,21] that  $a \approx -8.8$  eV. By contrast there are only few reports on experimental gradient-elastic tensors in GaAs [37,39,42] with only one series of experiments where  $S_{11}$  and  $S_{44}$  were measured

TABLE I. GaAs parameters.

Parameter	Units	This work	Previous work
$a = a_c + a_v$	eV		-8.7 [9]; -8.9 [10]; -8.7 [11]; -8.93 [12]; -8.72 [13]; -10.19 [14]; -8.33 [20]; -8.8 [21]
$b$	eV		-2.1 [9]; -1.96 [10]; -1.76 [12]; -2.00 [13]; -2.00 [14]; -2.0 [20]; -1.85 [21]
$b/a$		$0.242 \pm 0.008$	0.24 [9]; 0.22 [10]; 0.20 [12]; 0.23 [13]; 0.20 [14]; 0.24 [20]; 0.21 [21]
$c_{11}$	GPa		122.1 [20]; 118.8 [21]
$c_{12}$	GPa		56.6 [20]; 53.8 [21]
$c_{44}$	GPa		60.0 [20]; 59.4 [21]
$\frac{2c_{12}+c_{11}}{2c_{12}-2c_{11}}$			-1.796 [20]; -1.742 [21]
$\frac{Q^{69\text{Ga}} S_{11}^{69\text{Ga}}}{Q^{75\text{As}} S_{11}^{75\text{As}}}$		$-0.497 \pm 0.009$	-0.508 [39]
$Q^{75\text{As}} S_{11}^{75\text{As}}$	$10^{-6}$ V	+0.758	$\pm 1.06$ [39]
$Q^{69\text{Ga}} S_{11}^{69\text{Ga}}$	$10^{-6}$ V	-0.377	$\mp 0.543$ [39]
$Q^{69\text{Ga}}$	$10^{-28}$ m <sup>2</sup>		0.171 [64]
$Q^{75\text{As}}$	$10^{-28}$ m <sup>2</sup>		0.314 [64]
$S_{11}^{75\text{As}}$	$10^{21}$ V/m <sup>2</sup>	+24.2	$\pm 34.0$ [39]
$S_{11}^{69\text{Ga}}$	$10^{21}$ V/m <sup>2</sup>	-22.0	$\mp 31.7$ [39]

directly [38,39]. Thus we use  $a \approx -8.8$  eV [21] to evaluate  $Q^{75\text{As}} S_{11}^{75\text{As}} \approx +0.76$   $\mu\text{V}$ . The uncertainty of this estimate arising from the experimental uncertainty in  $k_{[110]}^+$  is only  $\pm 3\%$ , so the main error is likely to arise from the uncertainty in  $a$ , which is approximately  $\pm 5\%$  based on the spread of the values derived in different independent studies. Using the  $k_{69\text{Ga}/75\text{As}}$  ratio measured in Sec. IV C we also estimate  $Q^{69\text{Ga}} S_{11}^{69\text{Ga}} \approx -0.38$   $\mu\text{V}$  for  $^{69}\text{Ga}$  with a similar relative uncertainty. These values are  $\sim 30\%$  smaller than those derived by Sundfors [39] from the nuclear acoustic resonance measurements (Table I). We point out here that normally it is the  $Q S_{11}$  product and not  $S_{11}$  that is measured in NMR experiments and is used to predict the NMR spectra in strained semiconductor structures—the individual values for  $S_{ijkl}$  and  $Q$  are not accessible in conventional NMR measurements. Nonetheless, for the reference, we quote in Table I the  $S_{11}$  values derived in this work and those reported in Ref. [39], where in both cases we divided the measured  $Q S_{11}$  products by the most recent recommended values [64] of quadrupolar moments  $Q$ . For practical applications, it is preferable to use the  $Q S_{11}$  product values, or when using  $S_{ijkl}$  and  $Q$  separately, take their values from the same source. We also note that the  $S_{11}$  values in Ref. [39] are in the c.g.s. units of statcoulomb/cm<sup>3</sup> and are multiplied here by 2 997 924.580 to convert them to the SI units V/m<sup>2</sup>.

## V. DISCUSSION AND CONCLUSION

An important feature of this work is that elastic strain is probed optically through the spectral shifts in the free-exciton PL in bulk GaAs. This method offers certain advantages: there is no need to measure the stress or control precisely the size and the shape of the sample, moreover the strain can be

probed locally on a micrometer scale, so that modest strain inhomogeneities across the sample are not a limitation. The downside is that the accuracy of the measured strain is limited by the current uncertainty in the deformation potentials. On the other hand, the detection of the nuclear quadrupolar effects in this work is achieved in a most straightforward way—by measuring the quadrupolar splitting of the NMR spectral triplet. This is different from the previous studies on GaAs [38,39] where detection was rather indirect and relied on measuring the changes of the quality factors of mechanical resonances.

The  $\sim 30\%$  difference in the measured  $S_{11}$  values between this work and the work of Sundfors [38,39] appears to be too large to be attributed to the uncertainty in deformation potentials of GaAs. Contribution of the AlGaAs barriers to the QD NMR signal is unlikely to affect our derivations either: it has been found previously that the fraction of the electron wave function density in the barriers is small ( $\sim 10\%$ ) and nuclear spin polarization in the AlGaAs barriers is lower than in the GaAs volume of the dot [59]. More importantly, the presence of a small strain induced by lattice mismatch at the GaAs/AlGaAs interface [observed in Fig. 2(b) as a finite NMR quadrupolar splitting  $\nu_Q$  in an unstressed sample] suggests that the contribution of the AlGaAs barrier to the overall NMR spectrum must have  $\nu_Q$  different from that of the QD volume. This weak and spectrally shifted NMR signal of the AlGaAs barrier is then most likely eliminated by the line-shape fitting procedure used to derive  $\nu_Q$  of the GaAs volume of the dot. An electron occupying a quantum dot interacts with the nuclear spins, but the dominant effect is of magnetic origin (Knight field) and in GaAs/AlGaAs QDs leads to broadening and shifts of the NMR spectra on the order of tens of kHz [49]. Both the EFGs and the deformation of the lattice [67] induced by a

conduction band electron are small. Even these small effects are suppressed in our NMR measurements since the rf field is applied when QD is not illuminated and therefore does not contain charges. The neutral (empty) state is confirmed by observing that in most QDs the  $-1/2 \leftrightarrow +1/2$  NMR transition is narrow ( $<4$  kHz for  $^{75}\text{As}$ , and still resolution limited). In some individual QDs the  $-1/2 \leftrightarrow +1/2$  transition is broader (up to 10 kHz for  $^{75}\text{As}$ ) indicating intermittent occupation of the dot by electrons, but there is no systematic deviation of  $\nu_Q$  in such dots. Based on these observations we conclude that the difference in  $S_{11}$  between this work and the earlier nuclear acoustic resonance experiments is of systematic nature.

On the other hand, we note that our ratio of  $S_{11}$  for Ga and As is in remarkably good agreement with the previous result [38,39]. Moreover, it was pointed out by Sundfors [38] that his room temperature acoustic resonance measurements of  $S_{11}$  for  $^{115}\text{In}$  in InSb were notably larger than the corresponding  $S_{11}$  values obtained in two independent studies on InSb using static strain [34,37] at 77 K. One possibility is that all of the  $S_{ijkl}$  values reported in Refs. [38,39] were overestimated due to a systematic scaling error arising from a number of parameters that needed to be calibrated for acoustic resonance measurements. Moreover, the deviation in the results may arise from the fundamental differences in how nuclear spin system responds to static and dynamic (acoustic wave) strain, as well as from the temperature dependence—these aspects remain largely unexplored for GaAs, whereas studies on hexagonal metals reveal a  $\sim 10\%$ – $20\%$  variation of EFGs [44,68] for temperatures between 0 and 300 K.

The PL/NMR method for derivation of the gradient-elastic tensor reported here have potential to be extended further. For example, the  $S_{44}$  component of GaAs that was not probed here, can be measured. Such a measurement would require shear strain and magnetic field which is not parallel to one of the cubic axes (e.g., [001]). The GaAs/AlGaAs pair is unique since it permits nearly lattice matched epitaxial growth. As a result, external stress can induce deformations significantly exceeding the built-in strain, making it possible to use band gap shifts to gauge the strain. Application to other materials, e.g., InAs/GaAs quantum wells and dots may require alternative methods for probing the strain, such as x-ray diffraction.

For practical applications the  $Q_{S_{11}}$  for GaAs can be taken directly from the values measured here (Table I). Since GaAs and InAs were found previously to have very similar gradient elastic tensors [39], we recommend using the GaAs  $S_{11}$  values from Table I for InAs.

#### ACKNOWLEDGMENTS

The authors are grateful to Ceyhun Bulutay and Yongheng Huo for fruitful discussions. This work was supported by the EPSRC Programme Grant EP/N031776/1, the Linz Institute of Technology (LIT), and the Austrian Science Fund (FWF): P 29603. E.A.C. was supported by a University Research Fellowship from Royal Society.

#### APPENDIX: RELATION BETWEEN STRAIN AND NUCLEAR QUADRUPOLE EFFECTS

The second spatial derivatives of the electrostatic potential  $V(x, y, z)$  at the nuclear sites form a second rank symmetric

tensor  $V_{\alpha\beta} = \frac{\partial^2 V}{\partial \alpha \partial \beta}$  ( $\alpha, \beta = x, y, z$ ). Small deformation of a solid body is described via the second rank elastic strain tensor

$$\epsilon_{ij} = \frac{1}{2} \left( \frac{\partial u_i}{\partial x_j} + \frac{\partial u_j}{\partial x_i} \right) \quad (i, j = x, y, z), \quad (\text{A1})$$

where  $u_i$  are the components of the vector field of displacements  $\vec{u}(x, y, z)$  characterizing the deformation. In the limit of small deformation,  $V_{ij}$  is related to  $\epsilon_{kl}$  via

$$V_{ij} = \sum_{k,l} S_{ijkl} \epsilon_{kl} \quad (i, j, k, l = x, y, z), \quad (\text{A2})$$

where  $S_{ijkl}$  is a fourth rank ‘‘gradient-elastic’’ tensor. Not all of its 81 components are independent, and the number of independent parameters is greatly reduced further in crystal structures with high symmetry. In case of a zinc-blend crystal (cubic symmetry group  $T_d$ ) the nonvanishing elements of  $S_{ijkl}$  are [34]

$$\begin{aligned} S_{xxxx} &= S_{yyyy} = S_{zzzz}, \\ S_{yzyz} &= S_{zxzx} = S_{xyxy}, \\ S_{xxyy} &= S_{yyzz} = S_{zzxx} = S_{xxzz} = S_{zzyy} = S_{yyxx}. \end{aligned} \quad (\text{A3})$$

Moreover, since  $V_{ij}$  and  $\epsilon_{ij}$  are both symmetric, the gradient elastic tensor has an additional symmetry with respect to the pair of the first and second indices as well as to the pair of the third and fourth indices ( $S_{ijkl} = S_{jikl} = S_{ijlk} = S_{jilk}$ ). Thus in a coordinate frame aligned with the crystal axes  $x \parallel [100]$ ,  $y \parallel [010]$ ,  $z \parallel [001]$  there are in total 21 nonzero components and the tensor is fully characterized by three independent parameters  $S_{xxxx}$ ,  $S_{xxyy}$ , and  $S_{yzyz}$ . Taking into account the symmetries of  $S_{ijkl}$  we can evaluate Eq. (A2) to find the explicit expression for the electric field gradients:

$$\begin{aligned} V_1 &= V_{xx} = S_{xxxx} \epsilon_{xx} + S_{xxyy} (\epsilon_{yy} + \epsilon_{zz}) \\ &= S_{xxxx} [\epsilon_{xx} - (\epsilon_{yy} + \epsilon_{zz})/2], \\ V_2 &= V_{yy} = S_{xxxx} \epsilon_{yy} + S_{xxyy} (\epsilon_{xx} + \epsilon_{zz}) \\ &= S_{xxxx} [\epsilon_{yy} - (\epsilon_{xx} + \epsilon_{zz})/2], \\ V_3 &= V_{zz} = S_{xxxx} \epsilon_{zz} + S_{xxyy} (\epsilon_{xx} + \epsilon_{yy}) \\ &= S_{xxxx} [\epsilon_{zz} - (\epsilon_{xx} + \epsilon_{yy})/2], \\ V_4 &= V_{yz} = V_{zy} = 2S_{yzyz} \epsilon_{yz}, \\ V_5 &= V_{xz} = V_{zx} = 2S_{yzyz} \epsilon_{xz}, \\ V_6 &= V_{xy} = V_{yx} = 2S_{yzyz} \epsilon_{xy}, \end{aligned} \quad (\text{A4})$$

where the right-hand side parts of the first three equations were obtained by setting  $S_{xxyy} = -S_{xxxx}/2$ , which is a common convention to take into account the fact that only the traceless part of  $V_{ij}$  is observable in NMR [69]. We have also introduced EFG components  $V_m$  ( $m = 1..6$ ) in Voigt notation, using which we can rewrite Eq. (A4) as

$$\begin{aligned} V_1 &= S_{11} [\epsilon_1 - (\epsilon_2 + \epsilon_3)/2], \\ V_2 &= S_{11} [\epsilon_2 - (\epsilon_1 + \epsilon_3)/2], \\ V_3 &= S_{11} [\epsilon_3 - (\epsilon_1 + \epsilon_2)/2], \\ V_4 &= S_{44} \epsilon_4, \\ V_5 &= S_{44} \epsilon_5, \\ V_6 &= S_{44} \epsilon_6, \end{aligned} \quad (\text{A5})$$

where  $S_{11} = S_{xxxx}$  and  $S_{44} = S_{yzyz}$ . While Voigt notation simplifies the equations and is commonly accepted it needs to be used with care. Unlike  $S_{ijkl}$ , the  $2 \times 2$  matrix  $S_{mn}$  is not a tensor and does not follow the tensor transformation rules. One of the consequences of this is that the definition of the nondiagonal components of strain should include an additional factor of 2, so that  $\epsilon_4 = 2\epsilon_{yz}$ ,  $\epsilon_5 = 2\epsilon_{xz}$ ,  $\epsilon_6 = 2\epsilon_{xy}$ , while this factor of 2 is not needed in the definition of  $V_4$ ,  $V_5$ ,  $V_6$  [see Eq. (A4)]. A similar situation is encountered in the strain-stress relation  $\sigma_{ij} = \sum_{k,l=x,y,z} c_{ijkl}\epsilon_{kl}$  expressed in Voigt notation where the shear strains  $\epsilon_4$ ,  $\epsilon_5$ ,  $\epsilon_6$  require a factor of 2 in their definition, while there is no such factor for the stress components  $\sigma_4$ ,  $\sigma_5$ ,  $\sigma_6$  (see Chap. 10 in Ref. [70]).

The Hamiltonian  $\hat{H}_Q$  describing the interaction of the nucleus with spin  $I$  and quadrupolar moment  $Q$  with the electric field gradients is [71]

$$\hat{H}_Q = \frac{eQ}{6I(2I-1)h} \sum_{i,j=x,y,z} V_{ij} \left( \frac{3}{2} (\hat{I}_i \hat{I}_j + \hat{I}_j \hat{I}_i) - \delta_{ij} I^2 \right), \quad (\text{A6})$$

where  $e > 0$  is the elementary charge,  $h$  is the Planck constant,  $\delta_{ij}$  is Kronecker's delta,  $\hat{I}_i$  are spin operator components in Cartesian coordinates, and the Hamiltonian is in frequency units (Hz). Static magnetic field gives rise to the Zeeman Hamiltonian

$$\hat{H}_Z = -\frac{\gamma B_z}{2\pi} \hat{I}_z, \quad (\text{A7})$$

where  $\gamma$  is the nuclear gyromagnetic ratio, and we explicitly consider the case of the field  $B_z$  aligned along the  $z$  axis. For the spin-3/2 nuclei the total Hamiltonian  $H_Z + H_Q$  is a  $4 \times 4$  matrix and can in principle be diagonalized analytically to find the eigenstates.

A much simpler approximate solution can be found for the case of large magnetic field. In our experiments the effects induced by magnetic field (characterized by Larmor frequency  $>40$  MHz) are at least two orders of magnitude larger than the quadrupolar effects (characterized by quadrupolar shifts  $<0.4$  MHz). Thus with good accuracy quadrupolar effects can be treated as a perturbation, and to the first order we can omit all off-diagonal terms of

the total Hamiltonian [72]. The resulting eigenstates are the eigenstates of the  $\hat{I}_z$  operator with eigenenergies (in Hz units)

$$\begin{aligned} E_{-3/2} &= \frac{3\gamma B_z}{4\pi} + \frac{eQ}{4h} S_{11}\epsilon_b, \\ E_{-1/2} &= \frac{\gamma B_z}{4\pi} - \frac{eQ}{4h} S_{11}\epsilon_b, \\ E_{+1/2} &= -\frac{\gamma B_z}{4\pi} - \frac{eQ}{4h} S_{11}\epsilon_b, \\ E_{+3/2} &= -\frac{3\gamma B_z}{4\pi} + \frac{eQ}{4h} S_{11}\epsilon_b, \end{aligned} \quad (\text{A8})$$

where we have substituted the EFG values from Eq. (A4), the energies are indexed by their corresponding  $\hat{I}_z$  eigenvalue, and the effect of elastic deformation on the nuclear spin states is manifested only via the biaxial part of strain  $\epsilon_b = \epsilon_{zz} - (\epsilon_{xx} + \epsilon_{yy})/2$ . The dipolar transitions are allowed for the pairs of states where  $I_z$  changes by  $\pm 1$ , and the NMR frequencies are obtained by taking the differences of the corresponding energies in Eq. (A8):

$$\begin{aligned} \nu_{-3/2 \leftrightarrow -1/2} &= \frac{\gamma B_z}{2\pi} + \frac{eQ}{2h} S_{11}\epsilon_b, \\ \nu_{-1/2 \leftrightarrow +1/2} &= \frac{\gamma B_z}{2\pi}, \\ \nu_{+1/2 \leftrightarrow +3/2} &= \frac{\gamma B_z}{2\pi} - \frac{eQ}{2h} S_{11}\epsilon_b. \end{aligned} \quad (\text{A9})$$

Equations (A9) describe a triplet of NMR transitions with a central transition  $-1/2 \leftrightarrow +1/2$  and two satellite transitions on either side of the central transition, separated by the quadrupolar shift

$$\nu_Q = \frac{eQ}{2h} S_{11}\epsilon_b, \quad (\text{A10})$$

which is the same as Eq. (2). The frequency of the  $-1/2 \leftrightarrow +1/2$  transition is unaffected by quadrupolar interactions according to Eq. (A9) since we neglect here the small second order quadrupolar effects.

- 
- [1] S. L. Chuang, *Physics of Optoelectronic Devices* (Wiley, New York, 1995).
- [2] Y. Sun, S. E. Thompson, and T. Nishida, *Strain Effect in Semiconductors. Theory and Device Applications* (Springer, New York, 2010).
- [3] S. Seidl, M. Kroner, A. Högele, K. Karrai, R. J. Warburton, A. Badolato, and P. M. Petroff, *Appl. Phys. Lett.* **88**, 203113 (2006).
- [4] F. Ding, R. Singh, J. D. Plumhof, T. Zander, V. Křápek, Y. H. Chen, M. Benyoucef, V. Zwiller, K. Dörr, G. Bester, A. Rastelli, and O. G. Schmidt, *Phys. Rev. Lett.* **104**, 067405 (2010).
- [5] L. Seravalli, M. Minelli, P. Frigeri, P. Allegri, V. Avanzini, and S. Franchi, *Appl. Phys. Lett.* **82**, 2341 (2003).
- [6] R. Trotta, P. Atkinson, J. D. Plumhof, E. Zallo, R. O. Rezaev, S. Kumar, S. Baunack, J. R. Schroter, A. Rastelli, and O. G. Schmidt, *Adv. Mater.* **24**, 2668 (2012).
- [7] A. Rastelli, F. Ding, J. D. Plumhof, S. Kumar, R. Trotta, C. Deneke, A. Malachias, P. Atkinson, E. Zallo, T. Zander, A. Herklotz, R. Singh, V. Krapek, J. R. Schroter, S. Kiravittaya, M. Benyoucef, R. Hafenbrak, K. D. Jons, D. J. Thurmer, D. Grimm, G. Bester, K. Dorr, P. Michler, and O. G. Schmidt, *Phys. Status Solidi B* **249**, 687 (2011).
- [8] J. Martin-Sanchez, R. Trotta, A. Mariscal, R. Serna, G. Piredda, S. Stroj, J. Edlinger, C. Schimpf, J. Aberl, T. Lettner, J. Wildmann, H. Huang, X. Yuan, D. Ziss, J. Stangl, and A. Rastelli, *Semicond. Sci. Technol.* **33**, 013001 (2018).
- [9] F. H. Pollak, M. Cardona, and K. L. Shaklee, *Phys. Rev. Lett.* **16**, 942 (1966).
- [10] R. N. Bhargava and M. I. Nathan, *Phys. Rev.* **161**, 695 (1967).
- [11] R. Bendorius and A. Shileika, *Solid State Commun.* **8**, 1111 (1970).

- [12] M. Chandrasekhar and F. H. Pollak, *Phys. Rev. B* **15**, 2127 (1977).
- [13] H. Qiang, F. H. Pollak, and G. Hickman, *Solid State Commun.* **76**, 1087 (1990).
- [14] R. Mair, R. Prepost, E. Garwin, and T. Maruyama, *Phys. Lett. A* **239**, 277 (1998).
- [15] C. Priester, G. Allan, and M. Lannoo, *Phys. Rev. B* **37**, 8519 (1988).
- [16] C. G. Van de Walle, *Phys. Rev. B* **39**, 1871 (1989).
- [17] S.-H. Wei and A. Zunger, *Phys. Rev. B* **60**, 5404 (1999).
- [18] T. Cheiwchanamnganj and W. R. L. Lambrecht, *Phys. Rev. B* **84**, 035203 (2011).
- [19] A. Cakan, C. Sevik, and C. Bulutay, *J. Phys. D: Appl. Phys.* **49**, 085104 (2016).
- [20] I. Vurgaftman, J. R. Meyer, and L. R. Ram-Mohan, *J. Appl. Phys.* **89**, 5815 (2001).
- [21] S. Adachi, *Properties of Semiconductor Alloys: Group-IV, III-V and II-VI Semiconductors* (Wiley, New York, 2009).
- [22] E. A. Chekhovich, K. V. Kavokin, J. Puebla, A. B. Krysa, M. Hopkinson, A. D. Andreev, A. M. Sanchez, R. Beanland, M. S. Skolnick, and A. I. Tartakovskii, *Nat. Nanotechnol.* **7**, 646 (2012).
- [23] M. Munsch, G. Wust, A. V. Kuhlmann, F. Xue, A. Ludwig, D. Reuter, A. D. Wieck, M. Poggio, and R. J. Warburton, *Nat. Nanotechnol.* **9**, 671 (2014).
- [24] K. Flisinski, I. Y. Gerlovin, I. V. Ignatiev, M. Y. Petrov, S. Y. Verbin, D. R. Yakovlev, D. Reuter, A. D. Wieck, and M. Bayer, *Phys. Rev. B* **82**, 081308 (2010).
- [25] P. S. Sokolov, M. Y. Petrov, T. Mehrtens, K. Müller-Caspary, A. Rosenauer, D. Reuter, and A. D. Wieck, *Phys. Rev. B* **93**, 045301 (2016).
- [26] M. S. Kuznetsova, K. Flisinski, I. Y. Gerlovin, M. Y. Petrov, I. V. Ignatiev, S. Y. Verbin, D. R. Yakovlev, D. Reuter, A. D. Wieck, and M. Bayer, *Phys. Rev. B* **89**, 125304 (2014).
- [27] C. Bulutay, *Phys. Rev. B* **85**, 115313 (2012).
- [28] C. Bulutay, E. A. Chekhovich, and A. I. Tartakovskii, *Phys. Rev. B* **90**, 205425 (2014).
- [29] E. A. Chekhovich, M. Hopkinson, M. S. Skolnick, and A. I. Tartakovskii, *Nat. Commun.* **6**, 6348 (2015).
- [30] A. Bechtold, D. Rauch, F. Li, T. Simmet, P.-L. Ardetl, A. Regler, K. Müller, N. A. Sinitsyn, and J. J. Finley, *Nat. Phys.* **11**, 1005 (2015).
- [31] G. Wüst, M. Munsch, F. Maier, A. V. Kuhlmann, A. Ludwig, A. D. Wieck, D. Loss, M. Poggio, and R. J. Warburton, *Nat. Nanotechnol.* **11**, 885 (2016).
- [32] T. Botzem, R. P. G. McNeil, J.-M. Mol, D. Schuh, D. Bougeard, and H. Bluhm, *Nat. Commun.* **7**, 11170 (2016).
- [33] R. Stockill, C. Le Gall, C. Matthiesen, L. Huthmacher, E. Clarke, M. Hugues, and M. Atature, *Nat. Commun.* **7**, 12745 (2016).
- [34] R. G. Shulman, B. J. Wyluda, and P. W. Anderson, *Phys. Rev.* **107**, 953 (1957).
- [35] J. L. Marsh and P. A. Casabella, *Phys. Rev.* **150**, 546 (1966).
- [36] V. L. Bogdanov and V. V. Lemanov, *Fiz. Tverd. Tela* **9**, 469 (1967) [*Sov. Phys. Solid State* **9**, 357 (1967)].
- [37] V. L. Bogdanov and V. V. Lemanov, *Fiz. Tverd. Tela* **10**, 212 (1968) [*Sov. Phys. Solid State* **10**, 159 (1968)].
- [38] R. K. Sundfors, *Phys. Rev.* **177**, 1221 (1969).
- [39] R. K. Sundfors, *Phys. Rev. B* **10**, 4244 (1974).
- [40] R. K. Sundfors and R. K. Tsui, *Phys. Rev. B* **12**, 790 (1975).
- [41] R. K. Sundfors, R. K. Tsui, and C. Schwab, *Phys. Rev. B* **13**, 4504 (1976).
- [42] D. J. Guerrier and R. T. Harley, *Appl. Phys. Lett.* **70**, 1739 (1997).
- [43] C. Brusewitz, U. Vetter, and H. Hofsass, *J. Phys.: Condens. Matter* **27**, 055401 (2015).
- [44] D. Torumba, K. Parlinski, M. Rots, and S. Cottenier, *Phys. Rev. B* **74**, 144304 (2006).
- [45] Y. Abreu, C. Cruz, P. V. Espen, C. Pérez, I. Piñera, A. Leyva, and A. Cabal, *Solid State Commun.* **152**, 399 (2012).
- [46] G. M. Volkoff, H. E. Petch, and D. W. L. Smellie, *Can. J. Phys.* **30**, 270 (1952).
- [47] C. Heyn, A. Stemmann, T. Koppen, C. Strelow, T. Kipp, M. Grave, S. Mendach, and W. Hansen, *Appl. Phys. Lett.* **94**, 183113 (2009).
- [48] P. Atkinson, E. Zallo, and O. G. Schmidt, *J. Appl. Phys.* **112**, 054303 (2012).
- [49] M. N. Makhonin, E. A. Chekhovich, P. Senellart, A. Lemaître, M. S. Skolnick, and A. I. Tartakovskii, *Phys. Rev. B* **82**, 161309 (2010).
- [50] M. Gurioli, P. Borri, M. Colocci, M. Gulia, F. Rossi, E. Molinari, P. E. Selbmann, and P. Lugli, *Phys. Rev. B* **58**, R13403 (1998).
- [51] J. Shah, R. C. C. Leite, and R. E. Nahory, *Phys. Rev.* **184**, 811 (1969).
- [52] K. Kudo, Y. Makita, I. Takayasu, T. Nomura, T. Kobayashi, T. Izumi, and T. Matsumori, *J. Appl. Phys.* **59**, 888 (1986).
- [53] A. V. Gopal, R. Kumar, A. S. Vengurlekar, A. Bosacchi, S. Franchi, and L. N. Pfeiffer, *J. Appl. Phys.* **87**, 1858 (2000).
- [54] A. Amo, M. D. Martín, L. Viña, A. I. Toropov, and K. S. Zhuravlev, *Phys. Rev. B* **73**, 035205 (2006).
- [55] D. D. Sell, S. E. Stokowski, R. Dingle, and J. V. DiLorenzo, *Phys. Rev. B* **7**, 4568 (1973).
- [56] Y. El Khalifi, B. Gil, H. Mathieu, T. Fukunaga, and H. Nakashima, *Phys. Rev. B* **39**, 13533 (1989).
- [57] A. Ulhaq, Q. Duan, E. Zallo, F. Ding, O. G. Schmidt, A. I. Tartakovskii, M. S. Skolnick, and E. A. Chekhovich, *Phys. Rev. B* **93**, 165306 (2016).
- [58] M. J. Snelling, E. Blackwood, C. J. McDonagh, R. T. Harley, and C. T. B. Foxon, *Phys. Rev. B* **45**, 3922 (1992).
- [59] E. A. Chekhovich, A. Ulhaq, E. Zallo, F. Ding, O. G. Schmidt, and M. S. Skolnick, *Nat. Mater.* **16**, 982 (2017).
- [60] B. Urbaszek, X. Marie, T. Amand, O. Krebs, P. Voisin, P. Maletinsky, A. Högele, and A. Imamoglu, *Rev. Mod. Phys.* **85**, 79 (2013).
- [61] E. A. Chekhovich, M. N. Makhonin, A. I. Tartakovskii, A. Yacoby, H. Bluhm, K. C. Nowack, and L. M. K. Vandersypen, *Nat. Mater.* **12**, 494 (2013).
- [62] E. A. Chekhovich, M. M. Glazov, A. B. Krysa, M. Hopkinson, P. Senellart, A. Lemaître, M. S. Skolnick, and A. I. Tartakovskii, *Nat. Phys.* **9**, 74 (2013).
- [63] The amplitudes of the NMR peaks are not linearly proportional to the differences in the nuclear spin level populations, since the spectra were measured using an “inverse” NMR method [22]. However, the amplitudes still depend monotonically on population differences, so that the satellite transition with a larger amplitude corresponds to spin levels with a larger population difference. This is the case both for the  $\sigma^+$  and  $\sigma^-$  pump polarization as has been observed previously in Ref. [57].
- [64] N. Stone, *At. Data Nucl. Data Tables* **111–112**, 1 (2016).

- [65] J. Barber, *Elasticity* (Springer, Berlin, 2010).
- [66] R. I. Cottam and G. A. Saunders, *J. Phys. C: Solid State Phys.* **6**, 2105 (1973).
- [67] S. Tiemeyer, M. Bombeck, H. Göhring, M. Paulus, C. Sternemann, J. Nase, F. J. Wirkert, J. Möller, T. Büning, O. H. Seeck, D. Reuter, A. D. Wieck, M. Bayer, and M. Tolan, *Nanotechnology* **27**, 425702 (2016).
- [68] R. Raghavan and P. Raghavan, *Phys. Lett. A* **36**, 313 (1971).
- [69] R. J. Harrison and P. L. Sagalyn, *Phys. Rev.* **128**, 1630 (1962).
- [70] R. E. Newnham, *Properties of Materials. Anisotropy, Symmetry, Structure* (Oxford University Press, Oxford, 2005).
- [71] C. P. Slichter, *Principles of Magnetic Resonance* (Springer, Berlin, 1990).
- [72] R. V. Pound, *Phys. Rev.* **79**, 685 (1950).